Materials Chemistry and Physics 218 (2018) 18–27

Contents lists available at ScienceDirect

Materials Chemistry and Physics

journal homepage: www.elsevier.com/locate/matchemphys

Combined effects of multi-walled carbon nanotubes and lignin on polymer fiber-reinforcedepoxy composites

Panagiotis Goulis, Ioannis A. Kartsonakis, Konstantinos Mpalias, Costas Charitidis*

Research Unit of Advanced, Composite, Nano-Materials and Nanotechnology, School of Chemical Engineering, National Technical University of Athens, 9 Heroon Polytechniou St., Zographos, Athens, GR-15773, Greece

HIGHLIGHTS

- Synthesis of fibers including carbon nanotubes, lignin and nylon.
- Enhancement of the physical and thermal properties of the fibers and composites.
- Fiber reinforced epoxy composites demonstrated increased tolerance to stress.

GRAPHICAL ABSTRACT

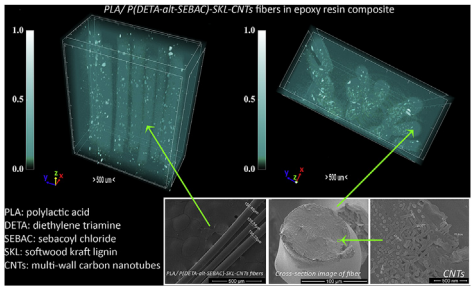

ARTICLE INFO

Keywords:
Lignin
MWCNTs
Fibers
Polymers
Composites

ABSTRACT

This study is focused on the manufacturing of cost effective fibers that can be used as durable reinforcing materials. Nylon aliphatic polymer was synthesized and conjugated with softwood kraft lignin, multi-wall carbon nanotubes as well as with commercial polymers such as poly(lactic acid) and polypropylene. After the synthesis, the materials were melt spun producing fibers that were characterized in respect of their morphology, structural, chemical and elemental composition. In addition, epoxy composites were manufactured, incorporating the aforementioned fibers, in order to assess their mechanical behavior via tensile testing. The produced composites exhibited improved mechanical properties in respect of ultimate tensile strength and elastic modulus. The fiber composites were synthesized via a simple method, which combines chemistry and engineering in a multi-stage experimental process.

1. Introduction

One of the dominant reasons for the high price of fiber reinforced polymers is the costly fabrication of the conventional polyacrylonitrile fiber precursors. A potential low cost fiber component candidate is lignin, a naturally abundant polymer that can be easily extracted from the cell wall of plants [1]. Lignin has several aromatic groups and a three-dimensional complex structure, which is not yet fully defined [2,3].

Another fiber component candidate is nylon. Regarding nylon, the most common type is nylon-6,6 which can be synthesized by adding sebacoyl chloride in an hexamethylene diamine solution. In addition, it has been successfully melt spun into filaments after been mixed with cellulose, as presented by Zhu et al. [4]. Nylon-6,6 has been effectively electrospun in combination with butylene terephthalate composites and characterized by An et al. [5]. Furthermore, McHenry and Stachurski have manufactured composite materials based on nylon fibers [6].

Taking into consideration that the demand for advanced, durable

* Corresponding author.
E-mail address: charitidis@chemeng.ntua.gr (C. Charitidis).

https://doi.org/10.1016/j.matchemphys.2018.07.025
Received 1 April 2018; Received in revised form 30 June 2018; Accepted 11 July 2018
Available online 12 July 2018
0254-0584/

and robust materials is becoming increasingly higher, a combination of lignin and nylon type polymers is evidenced as a feasible way to form spinnable composites with tailored properties and desirable chemical and physical behavior [7]. However, it may be remarked that the intolerable cost of these materials has always been a significant impediment to their quality enhancement. Under this heading, contemporary composite materials have been developed containing relatively low cost polymers, such as poly(lactic acid) (PLA), enriched with reinforcing compounds, like multi-wall carbon nanotubes (MWCNTs) [8,9]. Furthermore, incorporation of natural and green substances into composites has been attempted and the manufacturing processes have been thoroughly investigated [10,11].

The modification of composites using CNTs is widely investigated, due to their highly desired properties. The characteristics of these composites have been assessed and defined [12,13]. A combination of CNTs with other compounds has also been conducted in order to achieve even better properties and thermal stability [14,15]. Additionally, taking into consideration that the final goal of the synthesis and development of such materials is to produce fibers which can then be processed into carbon fibers with minimum cost, electro-spun [16], dry-spun and melt-spun fibers [17] have been also used towards that direction. Nevertheless, the mere blending of different compounds in order to produce a functional final product is not adequate [18]. Therefore, the optimization of all the included parameters is a factor of paramount importance [19] for the synthesis of a durable composite. Subsequently, the final material undergoes several characterization techniques, mechanical and physical trials in order to determine its durability, morphology, structure and potential [20–22].

The aim of this study was to design and produce cost effective polymeric fibers [23], with a diameter of micrometers, that can be used as durable reinforcing materials, via repeatable and applicable methods [24,25]. Therefore, melt-spun fibers containing nylon, MWCNTs, softwood kraft lignin (SKL) together with commercial polymers, either PLA or polypropylene (PP), were synthesized and characterized in respect of their morphology, structural, chemical and elemental composition. An evaluation of the MWCNTs addition into these blends was conducted with respect to fiber alignment. Moreover, an investigation of further SKL addition in the precursor blends was carried out with respect to the fibers surface texture, their total porosity, thickness and density. Finally, experiments were performed on composites based on epoxy resin including the aforementioned fibers regarding their total stress and strain tolerance. The motivation of this work was highlighted by the processes which lead to the exploitation of SKL, MWCNTs and nylon aliphatic polymer [1,26,27] in the view of producing cost-effective and usable products such as fibers, which can function as reinforcing materials in composites, [28,29].

2. Materials and methods

2.1. Materials

All chemicals were of analytical reagent grade. Polypropylene (PP, M_n ~67,000, Aldrich, St. Louis, USA), polylactic acid (PLA, M_w ~60,000, Aldrich, St. Louis, USA), hydrochloric acid (HCl 37%, Fisher Chemicals, Waltham, Massachusetts, USA), sebacoyl chloride (SEBAC, Acros Organics, Geel, Belgium), diethylene triamine (DETA, Fisher Chemicals, Waltham, Massachusetts, USA), acetylene (Air Liquide), Fe $(NO_3)_3{\cdot}9H_2O$ (Aldrich, St. Louis, USA), zeolite Y (Alfa Aesar; particle size ~1 μm; specific surface area 975 m^2/g), bisphenol-A/F monofunctional RD (ER 1042–7, Ipox Chemicals GmbH, Laupheim, Germany) and modified cycloaliphatic amine (EH 2117, Ipox Chemicals GmbH, Laupheim, Germany) were used as received without further purification. Softwood kraft lignin (SKL, Westvaco Corp., Indulin AT, MWV, Norcross, Georgia, USA) was treated with HCl 0.1 M prior to its use. All melt-spinning blends were dried in a vacuum oven for 24 h prior to their extrusion.

2.2. Experimental process

Synthesis of MWCNTs was performed according to our previous work [30] via chemical vapor deposition (CVD) method using a thermal reactor that consists of a horizontal quartz tube housed in a three-zone cylindrical furnace. Firstly, the catalyst particles [Fe/zeolite particles, Fe content (20 wt%)] were synthesized by dissolving appropriate amounts of zeolite and $Fe(NO_3)_3{\cdot}9H_2O$ in water. The obtained slurry was placed into tubes at 95 °C for 24 h. After that, the resulting dispersion was centrifuged at 2.0×10^3 rpm for 10 min, the supernatant solution was discarded and the obtained particles were dried at 120 °C for 4 h. Finally, the received material was calcinated at 550 °C under nitrogen flow for 1 h.

Subsequently, the produced catalyst was placed on a silicon substrate, located inside the quartz tube, in the middle of the reactor's isothermal zone. The system was purged from atmospheric air via argon flow through the quartz tube (flow rate 2.0×10^2 ml/min). Then, the reactor was heated at 800 °C. Afterwards, the argon was replaced with a mixture of gases (acetylene/argon 40:60) with a flow rate of 3.5×10^2 ml/min. The synthesis was carried out at the same temperature for 1 h, where pyrolysis of the acetylene took place and carbonaceous materials were deposited on the silicon substrate. The produced MWCNTs were cooled down to room temperature in inert atmosphere. Then, they were milled and exposed to atmospheric air flow at 400 °C for 1 h, in order to remove the amorphous carbon.

The obtained MWCNTs were purified from the catalyst metal particles via constant boiling with 5M HCl solution, in a Soxhlet extractor. Afterwards, the surface of the produced MWCNTs was functionalized with –COOH groups by using an acid solution mixture of nitric acid and sulfuric acid (HNO_3:H_2SO_4 1:3). The MWCNT/acid mixture (1.5×10^{-1} g MWCNTs/1.0×10^1 ml acid solution) was stirred for 5 h at room temperature. The treatment was followed by ice quenching and neutralization with an aquatic solution of NaOH. The suspension was filtered and the deposited on the filter black powder, was rinsed with distilled water, ethanol, acetone and distilled water. Finally, it was dried in an oven. The surface functionalization of the aforementioned MWCNTs with carboxylic groups was carried out in order to enhance their chemical affinity properties with diethylene triamine (DETA) and sebacoyl chloride (SEBAC).

The polymerization of DETA and SEBAC results to the synthesis of a nylon aliphatic type polymer, entitled *P(DETA-alt-SEBAC)*. Samples of nylon and nylon-SKL such as *P(DETA-alt-SEBAC)* and *P(DETA-alt-SEBAC)-SKL* were synthesized in order to investigate the differences between the nylon type polymer and the SKL enriched polymer. The SKL was purified prior its use with HCl 0.1 M. Afterwards, 2.0×10^1 ml of DETA and 1.0×10^1 ml of SEBAC were mixed into a glass spherical flask so as to produce the nylon type polymer *P(DETA-alt-SEBAC)*. The aforementioned chemical reactions are depicted in equations (1)–(3) (Fig. 1). Then, the produced material was oven dried at 80 °C. Furthermore, in another spherical glass flask, 2.0×10^1 ml of DETA and 2.0 g of SKL were mixed under stirring until the full dissolution of SKL. Subsequently, 1.0×10^1 ml of SEBAC was added to the reaction mixture and the SKL enriched nylon type polymer was formed, entitled *P(DETA-alt-SEBAC)-SKL*. The fabricated nylon type polymer was dried in an oven at 80 °C for 24 h. The mechanism of the esterification reaction (alcoholysis) between SKL and *P(DETA-alt-SEBAC)* is illustrated in the chemical reactions (4), (5) and (6) (Fig. 2). The esterification process comprises the formation of a tetrahedral intermediate due to an addition of oxygen (nucleophile) to the carbonyl group. Then, an electron pair from oxygen displaces the chloride (leaving group), yielding a new carbonyl compound as a product.

Moreover, *P(DETA-alt-SEBAC)-CNTs* and *P(DETA-alt-SEBAC)-SKL-CNTs* samples were also synthesized. Therefore, in a spherical glass flask, 5.0×10^{-1} g of MWCNTs were dissolved in 3.0×10^1 ml of DETA under stirring at room temperature. After that, 1.0×10^1 ml of SEBAC was added to the mixture so as to produce *P(DETA-alt-SEBAC)*

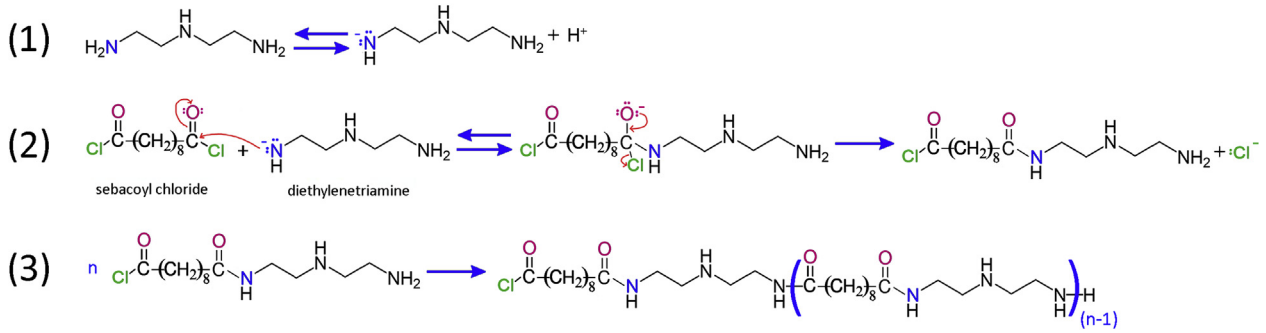

Fig. 1. Chemical equations of the reactions between diethylenetriamine and sebacoyl chloride.

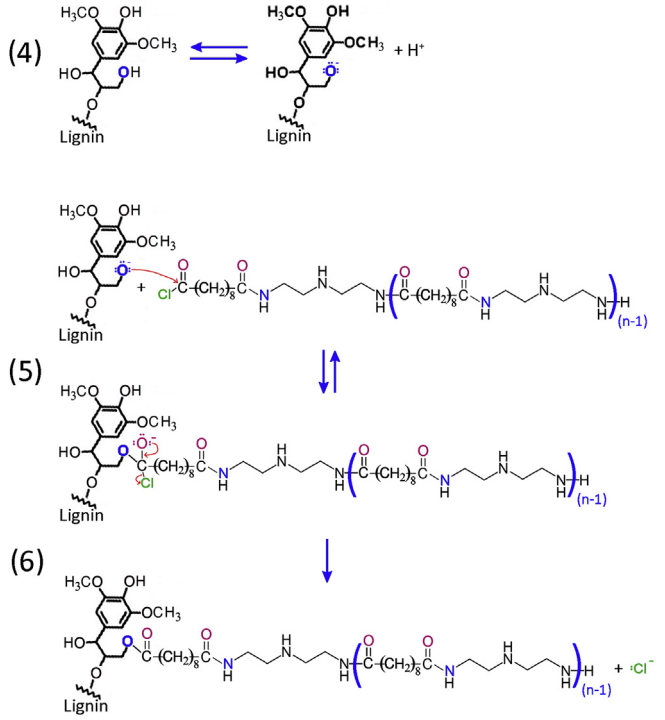

Fig. 2. Mechanism of the esterification reaction between lignin and the nylon polymer.

enriched in MWCNTs, entitled *P(DETA-alt-SEBAC)-CNTs*. The SEBAC addition is a very exothermic reaction, accomplished under vigorous manual stirring. After the completion of the reaction, the solid product was dried in an oven at 80 °C for 24 h.

In order to investigate the influence of SKL in this composite material, an additional experiment was conducted. In a spherical glass flask, 4.0×10^{-1} g of MWCNTs and 1.0×10^{1} g of SKL were dissolved in 5.0×10^{1}ml of DETA under vigorous stirring at room temperature. After the addition of 1.8×10^{1} ml of SEBAC into the reaction mixture, the nylon type polymer *P(DETA-alt-SEBAC)-SKL-CNTs* is fabricated. Finally, the polymer was oven dried at 80 °C.

2.3. Melt spinning

The aforementioned materials were melt spun, using a melt spinning apparatus (lab scale extruder), while mixed with pellets of the commercial polymers PLA and PP. The melted material was inserted in a cooled hopper where it dropped onto the hot surface of a cylindrical rotor. As the rotor turned, the material was dragged against the inclined surface of the stationary scroll and moved toward the outlet die. As the specimen was collected in the radial gap, it was compressed by the converging space between the scroll surface and the end of the header case.

The material was melted through heat conduction created by the mechanical work of the turning rotor and the temperature elevation. When sufficiently melted, the specimen moved to the axial gap where it was rotationally sheared between the end of the rotor and the inside of the case. This motion caused a centripetal pumping effect, enabling the specimen to flow to the outlet die and exit through the orifice. Commercial PLA and PP were purchased in pellets and were of relatively low molecular weight. Each extruded blend weighed 5.0 g. The maximum mass of the synthesized compound that could be achieved in the blend was 25 wt% (Supplementary Table 1). Beyond this percentage, it was not feasible for the blends to be easily treatable, or spinnable. The two commercial polymers, PLA and PP, were selected due to their spinning ability, known from previous experiments. The temperature range of the extrusion was 170 °C - 200 °C, while the roller distance from the extruder to the take-up system ranged between 4.7×10^{2} mm and 7.3×10^{2} mm, depending on each sample. The extrusion rate was adjusted, so that the wrapping of the fibers on the roller to be conducted in a controlled manner (Supplementary Table 2).

2.4. Characterization

The synthesized fibers were characterized in respect of their morphology and elemental composition via a Hitachi Tabletop Microscope TM3030 Scanning Electron Microscopy equipped with an Energy Dispersive X-Ray Spectrophotometer (EDS) system (QUANTAX 70) and an Ultra-High-Resolution Scanning Electron Microscopy (UHR-SEM) using NOVA NANOSEM 230 (FEI Company). Chemical analysis was conducted via Attenuated Total Reflectance Fourier Transform Infrared Spectroscopy (FT-IR) using a Cary 630 spectrometer (Agilent) with operating wavelength range at 4000-400 cm^{-1} at a resolution of 4 cm^{-1}.

The internal structural information of these samples was evaluated by a compact desk-top Bruker micro-CT, 3D X-ray scan system, SkyScan 1272. This system consists of a microfocus sealed X-ray source, which operates at 20–100 kV and 10 W (< 5 μm spot size @ 4 W), a 14bit cooled CCD fiber, which is optically coupled to a scintillator and an X-ray detector with a maximum resolution of 11 Mp (4032 × 2688 pixels). During the scan, the samples were mounted on a rotational stage. The distance between the rotation axis and the x-ray source was set from 6 mm to 12 mm and the pixel resolution was set to 2016 × 1344 in order to obtain reliable images. To ensure sufficient image resolution during CT acquisition process, the specimen was positioned in the scanner's field of view and the air surrounding the sample was excluded. The X-ray tube current was set to 40 lA and the X-ray tube voltage was set to 40 kV for all the samples. After the acquisition of the X-ray projection images, the 3D image was reconstructed by the image processing software of the X-ray CT system (NRecon). Multiple images were stacked through out-of-plane direction for each

specimen and used for image processing and calculations.

The thermal behavior of the aforementioned fibers was estimated via thermogravimetric analysis and differential scanning calorimetry (TGA/DSC) using a simultaneous TG-DTA/DSC Apparatus (STA 449 F5 Jupiter), at a heating rate of 20 °C/min in nitrogen atmosphere. A Dynisco LME (Laboratory Mixing Extruder) extruder which produces fibers, was used for the melt spinning experiments. The mechanical properties were investigated by tensile tests which were performed using a Zwicki 1120 apparatus, fitted with a 100N dynamometer at room temperature. The first step of the tensile test includes the tensile specimen formation according to ASTM D 2101-79 standard. A dumbbell type specimen consisting of epoxy resin, in which the fiber is embodied, is used for the experiment. Subsequently the specimen is inserted on the tensile machine's grapnels and the mechanical load is applied on the fiber.

3. Results and discussion

Taking into consideration the fibers production and characterization, several observations can be stated. Firstly, it should be mentioned that the fibers which did not contain SKL, presented agglomerates on their surface. This phenomenon indicates that these blends demonstrate neither sufficient spinning ability [7] nor compatibility with the commercial polymers PLA and PP. On the other hand, the fibers including SKL presented a reduced amount of agglomerates and their surface was macroscopically, smoother and thinner. It should be taken into account that the optimum results in respect of surface and porosity were observed for the fibers containing both SKL and MWCNTs. These samples demonstrated few agglomerates and an even smoother surface. The thinnest fiber was the one containing *P(DETA-alt-SEBAC)*, SKL, MWCNTs and PLA, that was also exhibited optimal performance in respect of stress tolerance.

Regarding the *P(DETA-alt-SEBAC)-CNTs* based fibers, it may be remarked that some agglomerates were observed on the fibers surface, possibly due to the incorporation of MWCNTs. This phenomenon indicates that these blends have neither sufficient spinning ability [31], nor sufficient compatibility with the commercial polymers. On the contrary, the *P(DETA-alt-SEBAC)-SKL-CNTs* based fibers had a smaller number of conglomerates and their surface was smoother and thinner macroscopically. It was observed that the miscibility of *P(DETA-alt-SEBAC)-CNTs* material with the commercial polymers PLA and PP was enhanced by the addition of SKL [32,33]. Finally, it was noticed that the miscibility of *P(DETA-alt-SEBAC)-SKL* material with the commercial polymers PLA and PP was improved by the addition of MWCNTs.

The thermal behavior (TGA/DSC) evaluation of the four produced samples (Table 1) via Thermogravimetric Analysis (TGA) and Differential Scanning Calorimetry (DSC) is illustrated in Fig. 3. Concerning this figure, it may be remarked that although the peak of the thermal degradation occurs at a relatively low temperature, the degradation proceeds slowly after that point, to higher temperature. According to the obtained TGA/DSC graphs, it can be concluded that the materials including MWCNTs present better thermal behavior compared to the other two samples. This result appears due to the fact that the initiation of their thermal degradation occurs at a higher temperature. Additionally, the mass residue is roughly 8% of the initial mass of the samples [34].

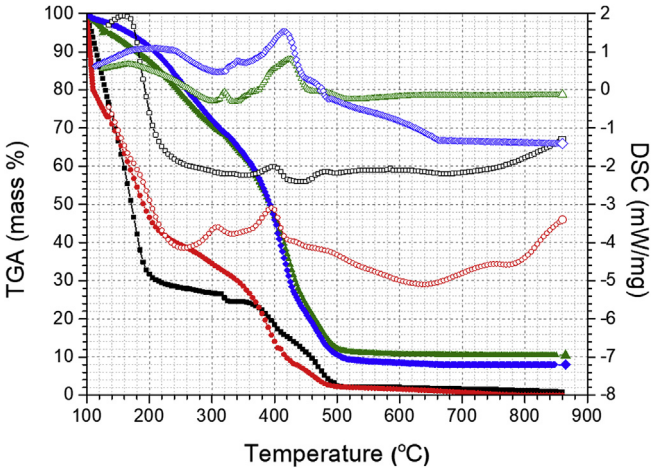

Fig. 3. TGA diagrams of: *P(DETA-alt-SEBAC)* (■), *P(DETA-alt-SEBAC)-SKL* (●), *P(DETA-alt-SEBAC)-CNTs* (▲) and *P(DETA-alt-SEBAC)-SKL-CNTs* (◆) samples. DSC diagrams of: *P(DETA-alt-SEBAC)* (□), *P(DETA-alt-SEBAC)-SKL* (○), *P(DETA-alt-SEBAC)-CNTs* (△) and *P(DETA-alt-SEBAC)-SKL-CNTs* (◇) samples.

Taking into account the TGA diagrams of *P(DETA-alt-SEBAC)-CNTs* and *P(DETA-alt-SEBAC)-SKL-CNTs* samples, it may be remarked that they slightly differ in respect of the temperature of their thermal degradation. More specifically, the SKL enriched sample delays the beginning of the decomposition as well as the temperature where the maximum rate of decomposition occurs. This outcome denotes that SKL incorporation results in the production of a sturdier material, at least at low temperatures [35]. However, both samples depict the same temperature of thermal degradation at 525 °C and lose roughly the same amount of mass, 90% and 92%, respectively. These phenomena suggest that fibers produced from these materials could be effectively thermal treated at temperatures below 500 °C, especially those enriched with SKL [36].

Regarding the DSC graphs, it can be mentioned, that samples *P(DETA-alt-SEBAC)-CNTs* and *P(DETA-alt-SEBAC)-SKL-CNTs* present transitions of a smaller range (wide curves) than the other two samples. This fact indicates that the thermal behavior of these two samples, and especially of the *P(DETA-alt-SEBAC)-SKL-CNTs,* is more gradual and controlled [37]. Also, the characteristic endothermic peak is more intense, meaning bigger heat capacity, which is also confirmed by the TGA graphs [38]. The thermal analysis results are demonstrated in Table 1.

As it is evidenced by the FT-IR diagram in Fig. 4, the graphs of *P(DETA-alt-SEBAC)* and *P(DETA-alt-SEBAC)-SKL* are similar. At about 3300 cm^{-1}, the relatively strong peak is ascribed to the N-H stretch of DETA. When SKL is added, the peak which corresponds to the O-H stretch of SKL hydroxyls appears at about 3200 cm^{-1} to 3300 cm^{-1} [39]. Thus, it is overlapped by the N-H stretch peak of DETA, because although some of the N-H bonds have become N-O- SKL bonds, there are other N-H bonds which have been sustained, due to the fact that some of the reactants have not successfully reacted. Moreover, the peak at 2910 cm^{-1} is assigned to the C-H stretch, so it is similar in both samples. Furthermore, the peak at 1650 cm^{-1} is ascribed to the C-C in-ring stretch (due to SKL) and to the C=O stretch [due to *P(DETA-alt-*

Table 1
Thermal analysis of the samples.

Sample	Start of thermal degradation (°C)	Peak of thermal degradation (°C)	End of thermal degradation (°C)	Mass Change (%)
P(DETA-alt-SEBAC)	60	185	520	−100
P(DETA-alt-SEBAC)-SKL	60	200	500	−100
P(DETA-alt-SEBAC)-CNTs	160	364	525	−90
P(DETA-alt-SEBAC)-SKL-CNTs	180	393	525	−92

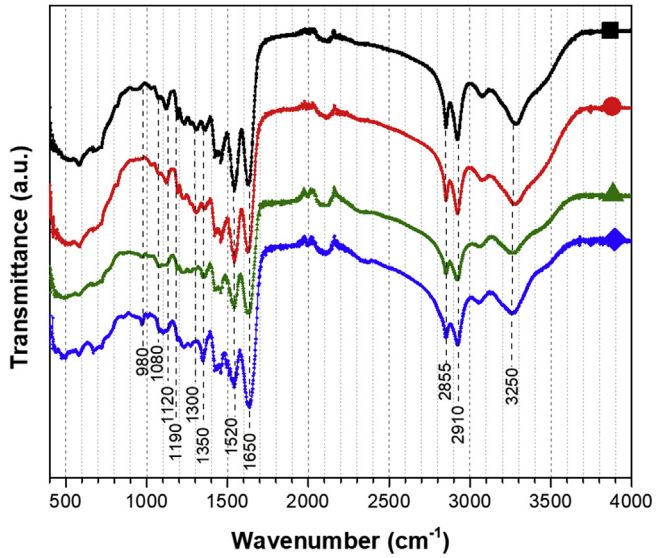

Fig. 4. FT-IR graphs of the *P(DETA-alt-SEBAC)* (■), *P(DETA-alt-SEBAC)-SKL* (●), *P(DETA-alt-SEBAC)-CNTs* (▲) and *P(DETA-alt-SEBAC)-SKL-CNTs* (◆) samples.

Table 2
FT-IR characteristic peaks of *P(DETA-alt-SEBAC)*, *P(DETA-alt-SEBAC)-SKL*, *P(DETA-alt-SEBAC)-CNTs* and *P(DETA-alt-SEBAC)-SKL-CNTs* samples.

Wavenumber (cm^{-1})	Type of bond
3300	N-H stretch
3250	aromatic C-H stretch, O-H stretch, N-H stretch
3200	O-H stretch
2910	C-H stretch, O-H stretch
2855	C-H stretch, N-H stretch
1650	C-C in-ring stretch, C=O stretch
1520	N-O asymmetric stretch
1300–1350	O-H deformation and C-O stretching vibration interaction of the ring, aromatic ethers
1120, 1190	C-N stretch
1080	CNT-COOH groups
980	C-H aromatic stretch

SEBAC)]. Additionally, the N-O asymmetric stretch is evident at 1500 cm^{-1}. Moreover, the peak at 1300 cm^{-1} is attributed to O-H deformation and C-O stretching ring vibration interaction of the aromatic ethers (due to SKL) and the secondary amides [due to *P(DETA-alt-SEBAC)*]. Considering the peak at 1300 cm^{-1} it may be remarked that it is more intense in the *P(DETA-alt-SEBAC)-SKL* sample compared to the sample without SKL, because of the presence of the aromatic rings and the aromatic ethers. Also, the peak at 1150 cm^{-1} is assigned to the C-N stretch of all materials [40]. To summarize, the characteristic wavenumbers and the peaks which are ascribed to them are demonstrated in Table 2.

The comparative FT-IR diagram of the two synthesized *P(DETA-alt-SEBAC)-SKL-CNTs* and *P(DETA-alt-SEBAC)-CNTs* materials is also demonstrated in Fig. 4. The peak at 1650 cm^{-1} is ascribed to the C-C in-ring stretch (due to SKL) and to the C=O stretch [due to *P(DETA-alt-SEBAC)*]. This peak is more intense for the *P(DETA-alt-SEBAC)-SKL-CNTs* sample, due to SKL presence, which amplifies the peak owing to its C-C in-ring bonds. Moreover, the peak at 2910 cm^{-1} is assigned to the C-H stretch of *P(DETA-alt-SEBAC)* and to the O-H stretch of SKL hydroxyls. This peak is slightly more intense for the SKL enriched sample, due to the stronger stretch of O-H SKL bonds which reinforce the peak. Furthermore, the small peak which can be noticed at 3250 cm^{-1} corresponds to the weak aromatic C-H stretch of SKL and the N-H stretch on account of the *P(DETA-alt-SEBAC)* [41]. The peak at

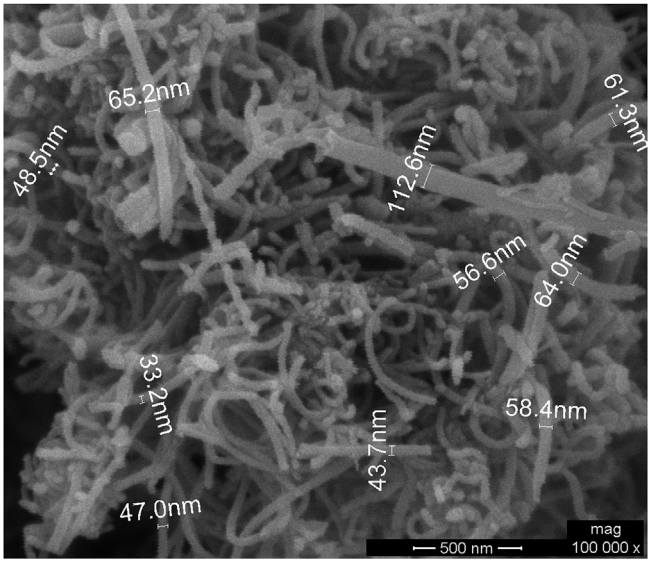

Fig. 5. SEM images of the fabricated MWCNTs.

1080 cm^{-1} is attributed to functionalized MWCNTs due to -COOH groups [42]. The peak at 980 cm^{-1} is assigned to C-H aromatic stretch [43]. The aforementioned FT-IR analysis results of the materials *P(DETA-alt-SEBAC)-SKL-MWCNTs* and *P(DETA-alt-SEBAC)-MWCNTs* are demonstrated in Table 2.

The SEM image of the fabricated MWCNTs is illustrated in Fig. 5. It can be observed that their diameters range between 30 nm and 113 nm. Concerning SEM analysis of the produced materials, it is evidenced that *PLA/P(DETA-alt-SEBAC)-SKL-CNTs* and *PP/P(DETA-alt-SEBAC)-SKL-CNTs* fibers are obtained via melt-spinning process (Figs. 6 and 7). Moreover, it may be remarked that smaller diameters are observed for PLA based fibers (134 ± 15 μm) compared to PP based fibers (158 ± 50 μm). This phenomenon suggests that SKL and MWCNTs are more miscible with PLA compared to PP in the extruded fiber, producing materials with possibly better mechanical and other properties [44,45]. The SEM cross-section images of the synthesized *PLA/P(DETA-alt-SEBAC)-SKL-CNTs* and *PP/P(DETA-alt-SEBAC)-SKL-CNTs* fibers are illustrated in Fig. 8a and c, respectively. Taking into account Fig. 8b and d, it is clearly denoted that MWCNTs have been successfully incorporated into the fibers.

Micro-CT images of *PLA/P(DETA-alt-SEBAC)-SKL-CNTs* and *PP/P(DETA-alt-SEBAC)-SKL-CNTs* fibers are illustrated in Fig. 9 [46]. In the case of PLA based fibers, as seen in Table 3, the SKL addition caused different results. As far as surface and thickness are concerned, they remained the same. In contrast, the structure linear density is reduced by a small amount, while the degree of anisotropy has been substantially increased. This fact indicates that the fibers became thinner but on the other hand the orientation was downgraded due to the SKL addition. This suggests that SKL is not fully compatible with PLA, thus miscibility between the two materials is not sufficient for proper compounding, when the MWCNTs are not also present [47]. The total porosity was decreased by a negligible amount.

Regarding the surface and thickness of PP based samples (Table 3), they demonstrate the same values with or without SKL, although the structure linear density is slightly increased by the SKL addition. Moreover, the degree of anisotropy is almost doubled after SKL incorporation, which indicates a great decrease in fibers orientation. This fact can be ascribed to the elongation ability, which the PP fibers present. Plain PP fibers tend to be elongated when subjected to tension, so when other compounds are mixed with PP pellets, it becomes more and more difficult for the fibers to retain their shape during extrusion. However, the most interesting result is the significant reduction of porosity from about 0.60% to 0.04%, which proves that SKL

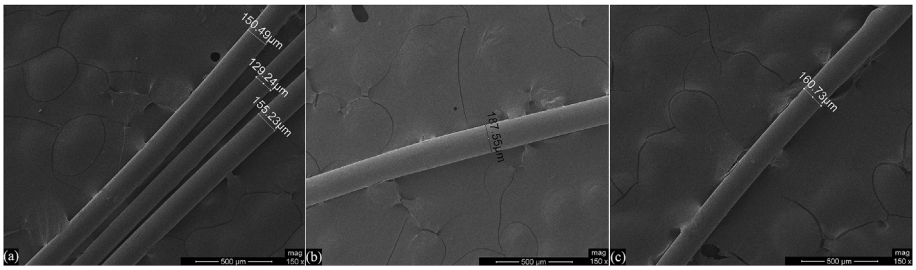

Fig. 6. SEM image of the fibers: (a) *PLA/P(DETA-alt-SEBAC)-SKL-CNTs*, (b) *PLA/P(DETA-alt-SEBAC)-SKL* and (c) *PLA/P(DETA-alt-SEBAC)-CNTs*.

incorporation produced a sturdier and more durable polymeric fiber [48].

It is evidenced that the materials' inner pores are reduced going from the *P(DETA-alt-SEBAC)-CNTs* to the *P(DETA-alt-SEBAC)-SKL-CNTs* fibers, regardless of the commercial polymer used. This fact results in a stronger and sturdier fiber due to SKL enrichment. It is also indicated that SKL and MWCNTs have an impact on fiber surface and morphology through crosslinking [49]. Furthermore, the thickness increases after SKL addition on a MWCNTs enriched material, denoting that the fiber surface becomes smoother, durable, and obtains enhanced properties. This indication is also reinforced by the object surface density, which remains stable in every occasion. Concerning the structure linear density, it may be noticed that it increases in value as the number of materials in each blend increases. On account of this phenomenon, it can be deduced that the irregular compounding of the materials in the holder of the extruder leads to a denser and maladjusted fiber surface [50].

According to micro-CT characterization, it can be noticed that the total porosity of all the produced fiber is below 2%. Furthermore, the derived fibers based on *P(DETA-alt-SEBAC)-SKL-CNTs* are thicker and denser than plain fibers based on *P(DETA-alt-SEBAC)*, a fact which suggests that the synthetic process results in the fabrication of a durable fiber. In addition, the degree of anisotropy is severely reduced after MWCNTs addition; this phenomenon suggests that the synthesis step is a decisive factor concerning fiber orientation. On the other hand, the SKL addition increased the degree of anisotropy, due to material miscibility issues.

In order to investigate the mechanical performance of the produced fibers as a reinforcing material, one-dimension epoxy composites were manufactured and tensile tests were performed. The produced fibers were placed inside dumbbell type sacrificial templates [51] and then an epoxy resin solution consisting of Bisphenol-A/F monofunctional RD (ER 1042–7) and modified cycloaliphatic amine (EH 2117) was added to each template and the specimens were left to cure overnight in room temperature. According to literature [52,53], after tensile tests, the sample orientation has not changed, an indication of possible further treatment. Furthermore, these values are similar to the tensile properties of natural fiber composites [54], while the difference in tensile strength between the fibers is ascribed to the different microstructure. The microstructure is affected by temperature, extrusion speed and materials residence time in the extrusion holder, while the size of the spinneret (diameter) also plays a significant role [55]. Additionally, the damage and tensile deformation of fibers are tremendously affected by both orientation and defects [56], while the chemical bonding has a strong impact on both the tensile strength and fiber stiffness [57].

Fig. 10 illustrates the f(strain) = stress diagrams of the produced composites, whereas Table 4 tabulates the corresponding results. It was evidenced via tensile tests, that the produced epoxy composites had advanced mechanical properties, due to fiber addition in the polymeric matrix. More specifically, the composites, which contained fibers enriched with MWCNTs, presented higher elastic modulus and ultimate tensile strength than composites containing only SKL fibers. Moreover, the composites including *PP/P(DETA-alt-SEBAC)-SKL-CNTs* fibers exhibited increased ultimate strength compared to the other composites containing PP fibers. However, a brittle behavior can also be observed that can be attributed to inhomogeneities between PP and *P(DETA-alt-SEBAC)*, SKL and MWCNTs. Inhomogeneities as well as the overall brittle behavior of PP based fibers compared to PLA based fibers were macroscopically observed during the melt spinning process. The optimum behavior was observed for the composite specimen containing the *PLA/P(DETA-alt-SEBAC)-SKL-CNTs* fibers.

Micro-CT images of the fibers inside the composites are demonstrated in Fig. 11 and the corresponding analysis is presented in Table 5. Although both of the composites exhibit similar values, it can be observed, that the composite which includes PLA fibers presents lower porosity and higher thickness, while PLA fibers demonstrate better dispersion and orientation into the resin matrix (possibly due to their thinness and smaller diameters). Another reason for that, is the better affinity of epoxy resin with PLA compared to PP. This phenomenon is ascribed to the -C = O and -OH groups, which are not present in the PP chain. Subsequently, these results are in accordance with the outcome of the tensile tests.

According to literature, it may be remarked that in the work of Wang et al. [14] carbon fibers with lignin and CNTs have been manufactured showing superior thermal stability compared to those manufactured in our work. Furthermore, in the work of Xu et al. [58] carbon fibers from CNTs grafted with lignin were produced and investigated for their mechanical tolerance. However, it should be taken into deep consideration that the fibers in the work of both Wang et al. [14] and Xu et al. [58] have not been investigated concerning their behavior in composites and their mechanical properties. Additionally, despite the fact that lignin has been investigated for the production of specific types

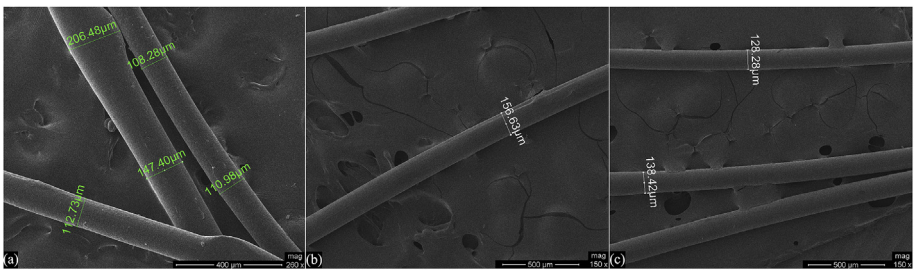

Fig. 7. SEM images of the fibers: (a) *PP/P(DETA-alt-SEBAC)-SKL-CNTs*, (b) *PP/P(DETA-alt-SEBAC)-SKL* and (c) *PP/P(DETA-alt-SEBAC)-CNTs*.

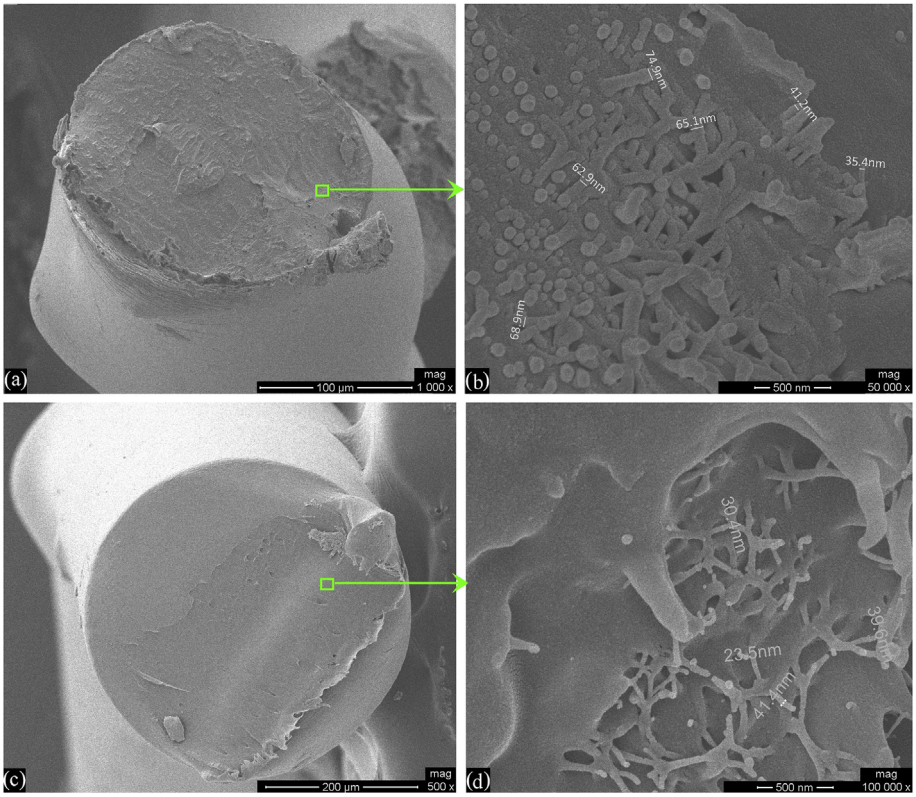

Fig. 8. The SEM cross-section images of the synthesized (a, b) *PLA/P(DETA-alt-SEBAC)-SKL-CNTs* and (c, d) *PP/P(DETA-alt-SEBAC)-SKL-CNTs* fibers.

of resin [59], it has not been referred for lignin to be used in a complex material along with commercial epoxy resins in order to form composites.

It should be taken into account that in this study, SKL, CNTs and *P(DETA-alt-SEBAC)* have been utilized to produce chemical compounds, which are successfully used in an emerging application [60,61]. The produced fibers were positioned in-plane and parallel into the epoxy resin mold, so as to ensure that they have the maximum effect to the composites behavior [62]. The obtained results in our work revealed that the tensile strength of the fabricated epoxy composites (Table 4) has the same order of magnitude as the tensile strength in the following work: Kenaf fiber/multi-walled carbon nanotube/polylactic acid green composites of P-Y. Chen et al. [8], poly(l-lactic acid)/ramie fabric biocomposites of D. Chen et al. [63] and polypropylene-glass fiber/carbon fiber hybrid composites of X. Yan and S. Cao [64]. In the work of Xu et al. [65], the produced hemp fibers reinforced composites demonstrated similar values of tensile strength, but their elastic modulus was of one order of magnitude less than in our work. On the other hand, in the work of Zegaoui et al. related to alkali modified hemp fibers reinforced cyanate ester/benzoxazine blend composites [66], the illustrated tensile strength and elastic modulus are higher than those in our study; however, it should be mentioned that the used pristine hemp fibers were commercial with enhanced initial tensile strength and no information is given in respect of their diameter.

To sum up, taking into account the obtained results and the literature, it may be remarked that the incorporation of *P(DETA-alt-SEBAC)*, SKL and MWCNTs into the fiber structure influenced the fibers mechanical properties, while the process was kept as simple as possible. The incorporation of both SKL and MWCNTs in a melt spun fiber, containing both a commercial and a chemically synthesized nylon [*P(DETA-alt-SEBAC)*] aliphatic polymer is a new attempt. Moreover, the specific chemical synthesis that was followed, leads to the successful conjugation of SKL, MWCNTs and *P(DETA-alt-SEBAC)* polymer before the materials enter the extruder. This experimental path ensures that the material is homogenized and that there will be no impediments, regarding the treatment and compatibility or miscibility of the materials during the extrusion step. In addition, the synthesis of this specific polymeric structure is a simple experimental path, towards the manufacturing of a low-cost fiber with desired properties.

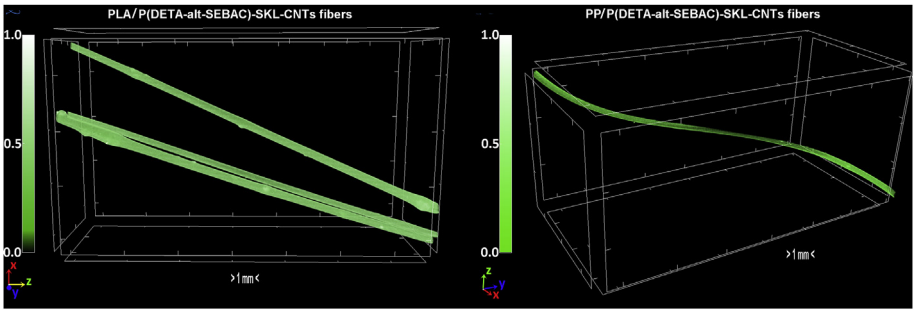

Fig. 9. Micro-CT images of the *PLA/P(DETA-alt-SEBAC)-SKL-CNTs* and *PP/P(DETA-alt-SEBAC)-SKL-CNTs* fibers.

Table 3
Micro-CT arithmetical results for the PLA and PP based fibers.

Parameters	*PLA-P(DETA-alt-SEBAC)*	*PLA-P(DETA-alt-SEBAC)-CNTs*	*PLA-P(DETA-alt-SEBAC)-SKL-CNTs*
Object Surface to Volume ratio	11.81	44.94	42.82
Object Surface Density (mm^{-1})	11.81	44.93	42.81
Structure Thickness (mm)	0.487	0.112	0.120
Structure Separation (mm)	0.026	0.012	0.012
Structure Linear Density (mm^{-1})	2.055	8.936	8.329
Degree of Anisotropy	3.436	2.505	3.596
Fractal Dimension	1.899	1.726	1.791
Total Porosity (%)	0.001	0.029	0.019
Parameters	*PP-P(DETA-alt-SEBAC)*	*PP-P(DETA-alt-SEBAC)-CNTs*	*PP-P(DETA-alt-SEBAC)-SKL-CNTs*
Object Surface to Volume ratio	13.80	38.65	38.92
Object Surface Density (mm^{-1})	13.80	38.43	38.90
Structure Thickness (mm)	0.306	0.089	0.092
Structure Separation (mm)	0.020	0.014	0.012
Structure Linear Density (mm^{-1})	3.268	11.19	12.82
Degree of Anisotropy	2.632	1.800	3.217
Fractal Dimension	1.890	1.759	1.669
Total Porosity (%)	0.016	0.563	0.042

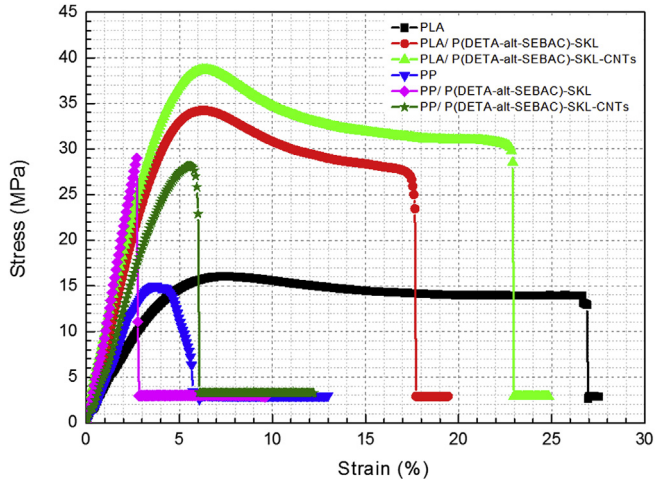

Fig. 10. Tensile test of the dumbbell fiber - epoxy composites, with PLA and PP based fibers.

Table 4
Tensile stretch arithmetical results for the PLA and PP based fibers.

Parameters	PLA	*PLA-P(DETA-alt-SEBAC)-SKL*	*PLA-P(DETA-alt-SEBAC)-SKL-CNTs*
Average E – Elasticity Modulus (MPa)	413	841	1020
max ε – Deformation Factor (Strain, %)	53.55	19.44	24.84
max σ – Ultimate Tensile Strength (Stress, MPa)	16	34.2	38.7
Test Speed (mm/min)	0.9	1.0	1.2
Lo – Length of Specimen (mm)	29	29	29
a – Height of Specimen (mm)	1.6	1.6	1.6
b – Width of Specimen (mm)	4.7	4.7	4.7
$A = a*b$ (mm^2)	7.52	7.52	7.52
Parameters	PP	*PP-P(DETA-alt-SEBAC)-SKL*	*PP-P(DETA-alt-SEBAC)-SKL-CNTs*
Average E – Elasticity Modulus (MPa)	499	975	628
max ε – Deformation Factor (Strain, %)	18.28	9.67	12.22
max σ – Ultimate Tensile Strength (Stress, MPa)	15	29	28.1
Test Speed (mm/min)	1.2	1.0	1.2
Lo – Length of Specimen (mm)	29	29	29
a – Height of Specimen (mm)	1.6	1.6	1.6
b – Width of Specimen (mm)	4.7	4.7	4.7
$A = a*b$ (mm^2)	7.52	7.52	7.52

4. Conclusions

In this study, polymer fibers were fabricated via the incorporation of SKL, MWCNTs, and *P(DETA-alt-SEBAC)* into commercial polymers, such as PLA and PP. The influence of all the aforementioned components was investigated in respect of the spinning ability, thermal behavior as well as homogeneity and mechanical properties of the fibers. The obtained results revealed that the combination of SKL and MWCNTs improved the produced fibers in terms of thermal stability and homogeneity. Furthermore, SKL caused better miscibility and compatibility of the different compounds at the time of extrusion. It was observed that PP produced thicker fibers with agglomerations and a more rugged surface than PLA.

The incorporation of the obtained fibers into epoxy resin composites, revealed that SKL enhanced the strength and tensile resistance of those composites, while MWCNTs improved them even more; the incorporation of *PLA/P(DETA-alt-SEBAC)-SKL-CNTs* fibers into epoxy coatings presented the best mechanical behavior. Concerning the initial aim, the outcome was the enhancement of the composites durability using modified fibers containing chemically synthesized material, in comparison to the plain fiber composites, as evidenced by the tensile testing. Finally, the obtained results confirmed the initial aim of this study to employ easily accessible compounds, so as to form cost effective materials via repeatable and applicable methods. Future plans include an increase of the percentage of the synthesized materials in the final product and the transformation of these fibers into carbon fibers. Then, they will be used to reinforce composites (resin composites, building materials, cement) and will be studied as to their effect on the mechanical properties, in comparison with the current results.

Acknowledgements

This work was supported by the EU FP7 Project “Functionalized Innovative Carbon Fibres Developed from Novel Precursors with Cost Efficiency and Tailored Properties” (FIBRALSPEC) under Grant Agreement no. 604248.

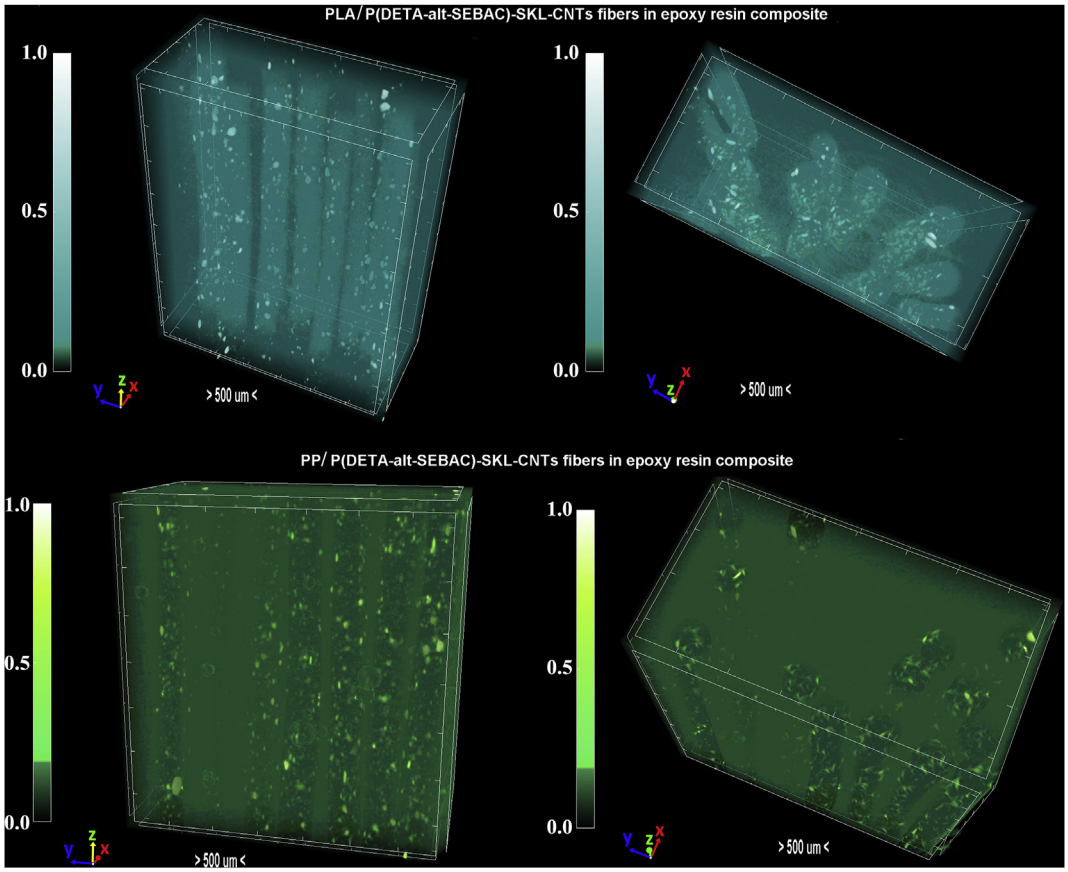

Fig. 11. Micro-CT images of *PLA/P(DETA-alt-SEBAC)-SKL-CNTs* and *PP/P(DETA-alt-SEBAC)-SKL-CNTs* fibers into epoxy resin composites.

Table 5
Micro-CT arithmetical results for the *PP/P(DETA-alt-SEBAC)-SKL-CNTs* and the *PLA/P(DETA-alt-SEBAC)-SKL-CNTs* fiber composites.

Parameters	*PP/P(DETA-alt-SEBAC)-SKL-CNTs* fiber composite	*PLA/P(DETA-alt-SEBAC)-SKL-CNTs* fiber composite
Object Surface to Volume ratio	3.585	2.839
Object Surface Density (mm^{-1})	3.570	2.832
Structure Thickness (mm)	0.740	0.833
Structure Separation (mm)	0.042	0.074
Structure Linear Density (mm^{-1})	1.346	1.197
Degree of Anisotropy	2.169	1.899
Fractal Dimension	2.258	2.220
Total Porosity (%)	0.406	0.236

Appendix A. Supplementary data

Supplementary data related to this article can be found at https://doi.org/10.1016/j.matchemphys.2018.07.025.

References

[1] M. Holmes, Lowering the cost of carbon fiber, Reinforc Plast 61 (2017) 279–283.
[2] N. Meek, D. Penumadu, O. Hosseinaei, D. Harper, S. Young, T. Rials, Synthesis and characterization of lignin carbon fiber and composites, Compos. Sci. Technol. 137 (2016) 60–68.
[3] A. Duval, M. Lawoko, A review on lignin-based polymeric, micro- and nano-structured materials, React. Funct. Polym. 85 (2014) 78–96.
[4] R. Zhu, V. Yadama, H. Liu, R.J.T. Lin, D.P. Harper, Fabrication and characterization of Nylon 6/cellulose nanofibrils melt-spun nanocomposite filaments, Compos. Appl. Sci. Manuf. 97 (2017) 111–119.
[5] T. An, B. Pant, S.Y. Kim, M. Park, S.-J. Park, H.-Y. Kim, Mechanical and optical properties of electrospun nylon-6,6 nanofiber reinforced cyclic butylene terephthalate composites, J. Ind. Eng. Chem. 55 (2017) 35–39.
[6] E. McHenry, Z.H. Stachurski, Composite materials based on wood and nylon fibre, Compos. Appl. Sci. Manuf. 34 (2003) 171–181.
[7] D. Kun, B. Pukánszky, Polymer/lignin blends: interactions, properties, applications, Eur. Polym. J. 93 (2017) 618–641.
[8] P.-Y. Chen, H.-Y. Lian, Y.-F. Shih, S.-M. Chen-Wei, R.-J. Jeng, Preparation, characterization and crystallization kinetics of Kenaf fiber/multi-walled carbon nanotube/polylactic acid (PLA) green composites, Mater. Chem. Phys. 196 (2017) 249–255.
[9] E. Wollan, Glass & carbon fiber reinforcement combine in hybrid long fiber thermoplastic composites to bridge price & performance gap, Reinforc Plast 61 (2017) 55–57.
[10] M.-p. Ho, H. Wang, J.-H. Lee, C.-k. Ho, K.-t. Lau, J. Leng, D. Hui, Critical factors on manufacturing processes of natural fibre composites, Compos. B Eng. 43 (2012) 3549–3562.
[11] A. Elkhaoulani, F.Z. Arrakhiz, K. Benmoussa, R. Bouhfid, A. Qaiss, Mechanical and thermal properties of polymer composite based on natural fibers: moroccan hemp fibers/polypropylene, Mater. Des. 49 (2013) 203–208.
[12] S. Bose, R.A. Khare, P. Moldenaers, Assessing the strengths and weaknesses of various types of pre-treatments of carbon nanotubes on the properties of polymer/carbon nanotubes composites: a critical review, Polymer 51 (2010) 975–993.
[13] J.K.W. Sandler, S. Pegel, M. Cadek, F. Gojny, M. van Es, J. Lohmar, W.J. Blau, K. Schulte, A.H. Windle, M.S.P. Shaffer, A comparative study of melt spun polyamide-12 fibres reinforced with carbon nanotubes and nanofibres, Polymer 45 (2004) 2001–2015.
[14] X. Xu, J. Zhou, L. Jiang, G. Lubineau, S.A. Payne, D. Gutschmidt, Lignin-based carbon fibers: carbon nanotube decoration and superior thermal stability, Carbon 80 (2014) 91–102.
[15] M.H. Al-Saleh, Electrically conductive carbon nanotube/polypropylene nanocomposite with improved mechanical properties, Mater. Des. 85 (2015) 76–81.

[16] J. Jin, B.-j. Yu, Z.-q. Shi, C.-y. Wang, C.-b. Chong, Lignin-based electrospun carbon nanofibrous webs as free-standing and binder-free electrodes for sodium ion batteries, J. Power Sources 272 (2014) 800–807.
[17] R. Hufenus, L. Gottardo, A.A. Leal, A. Zemp, K. Heutschi, P. Schuetz, V.R. Meyer, M. Heuberger, Melt-spun polymer fibers with liquid core exhibit enhanced mechanical damping, Mater. Des. 110 (2016) 685–692.
[18] A.-T. Chien, P.V. Gulgunje, H.G. Chae, A.S. Joshi, J. Moon, B. Feng, G.P. Peterson, S. Kumar, Functional polymer–polymer/carbon nanotube bi-component fibers, Polymer 54 (2013) 6210–6217.
[19] L. Feng, K. Li, B. Xue, Q. Fu, L. Zhang, Optimizing matrix and fiber/matrix interface to achieve combination of strength, ductility and toughness in carbon nanotube-reinforced carbon/carbon composites, Mater. Des. 113 (2017) 9–16.
[20] M. Mehdikhani, A. Matveeva, M.A. Aravand, B.L. Wardle, S.V. Lomov, L. Gorbatikh, Strain mapping at the micro-scale in hierarchical polymer composites with aligned carbon nanotube grafted fibers, Compos. Sci. Technol. 137 (2016) 24–34.
[21] A.A. Pérez-Fonseca, J.R. Robledo-Ortíz, D.E. Ramirez-Arreola, P. Ortega-Gudiño, D. Rodrigue, R. González-Núñez, Effect of hybridization on the physical and mechanical properties of high density polyethylene–(pine/agave) composites, Mater. Des. 64 (2014) 35–43.
[22] E. Părpăriţă, R.N. Darie, C.-M. Popescu, M.A. Uddin, C. Vasile, Structure–morphology–mechanical properties relationship of some polypropylene/lignocellulosic composites, Mater. Des. 56 (2014) 763–772 (1980-2015).
[23] J. Meredith, E. Bilson, R. Powe, E. Collings, K. Kirwan, A performance versus cost analysis of prepreg carbon fibre epoxy energy absorption structures, Compos. Struct. 124 (2015) 206–213.
[24] J.L. Espinoza-Acosta, P.I. Torres-Chávez, J.L. Olmedo-Martínez, A. Vega-Rios, S. Flores-Gallardo, E.A. Zaragoza-Contreras, Lignin in storage and renewable energy applications: a review, Journal of Energy Chemistry (2018), https://doi.org/10.1016/j.jechem.2018.02.015 (in press).
[25] F.H.M. Graichen, W.J. Grigsby, S.J. Hill, L.G. Raymond, M. Sanglard, D.A. Smith, G.J. Thorlby, K.M. Torr, J.M. Warnes, Yes, we can make money out of lignin and other bio-based resources, Ind. Crop. Prod. 106 (2017) 74–85.
[26] M.N. Alam, L.P. Christopher, A novel, cost-effective and eco-friendly method for preparation of textile fibers from cellulosic pulps, Carbohydr. Polym. 173 (2017) 253–258.
[27] E. Ibraim, J.-F. Camenen, A. Diambra, K. Kairelis, L. Visockaite, N.C. Consoli, Energy efficiency of fibre reinforced soil formation at small element scale: laboratory and numerical investigation, Geotext. Geomembranes 46 (2018) 497–510.
[28] H. Mainka, O. Täger, E. Körner, L. Hilfert, S. Busse, F.T. Edelmann, A.S. Herrmann, Lignin – an alternative precursor for sustainable and cost-effective automotive carbon fiber, Journal of Materials Research and Technology 4 (2015) 283–296.
[29] M. Akhshik, S. Panthapulakkal, J. Tjong, M. Sain, Life cycle assessment and cost analysis of hybrid fiber-reinforced engine beauty cover in comparison with glass fiber-reinforced counterpart, Environ. Impact Assess. Rev. 65 (2017) 111–117.
[30] A.-F.A. Trompeta, E.P. Koumoulos, I.A. Kartsonakis, C.A. Charitidis, Advanced characterization of by-product carbon film obtained by thermal chemical vapor deposition during CNT manufacturing, Manuf. Rev. 4 (7) (2017).
[31] A. Naseem, S. Tabasum, K.M. Zia, M. Zuber, M. Ali, A. Noreen, Lignin-derivatives based polymers, blends and composites: a review, Int. J. Biol. Macromol. 93 (2016) 296–313.
[32] O. Gordobil, I. Egüés, R. Llano-Ponte, J. Labidi, Physicochemical properties of PLA lignin blends, Polym. Degrad. Stabil. 108 (2014) 330–338.
[33] L. Dehne, C. Vila Babarro, B. Saake, K.U. Schwarz, Influence of lignin source and esterification on properties of lignin-polyethylene blends, Ind. Crop. Prod. 86 (2016) 320–328.
[34] J.E.K. Schawe, Remarks regarding the determination of the initial crystallinity by temperature modulated DSC, Thermochim. Acta 657 (2017) 151–155.
[35] A.K. Tripathi, J.G. Tsavalas, D.C. Sundberg, Quantitative measurements of the extent of phase separation during and after polymerization in polymer composites using DSC, Thermochim. Acta 568 (2013) 20–30.
[36] Q. Ouyang, X. Wang, X. Wang, J. Huang, X. Huang, Y. Chen, Simultaneous DSC/TG analysis on the thermal behavior of PAN polymers prepared by aqueous free-radical polymerization, Polym. Degrad. Stabil. 130 (2016) 320–327.
[37] M. Grochowicz, A. Kierys, TG/DSC/FTIR studies on the oxidative decomposition of polymer-silica composites loaded with sodium ibuprofen, Polym. Degrad. Stabil. 138 (2017) 151–160.
[38] A. Toda, M. Konishi, An evaluation of thermal lags of fast-scan microchip DSC with polymer film samples, Thermochim. Acta 589 (2014) 262–269.
[39] M. Ravindar Reddy, A.R. Subrahmanyam, M. Maheshwar Reddy, J. Siva Kumar, V. Kamalaker, M. Jaipal Reddy, X-RD, SEM, FT-IR, DSC studies of polymer blend films of PMMA and PEO, Mater. Today: Proceedings 3 (2016) 3713–3718.
[40] W. Jin, D. Shen, Q. Liu, R. Xiao, Evaluation of the co-pyrolysis of lignin with plastic polymers by TG-FTIR and Py-GC/MS, Polym. Degrad. Stabil. 133 (2016) 65–74.
[41] J. Zhao, W. Xiuwen, J. Hu, Q. Liu, D. Shen, R. Xiao, Thermal degradation of softwood lignin and hardwood lignin by TG-FTIR and Py-GC/MS, Polym. Degrad. Stabil. 108 (2014) 133–138.
[42] V. Tucureanu, A. Matei, A.M. Avram, FTIR spectroscopy for carbon family study, Crit. Rev. Anal. Chem. 46 (2016) 502–520.
[43] Y. Li, Z. Cai, M. Liao, J. Long, W. Zhao, Y. Chen, X. Li, Catalytic depolymerization of organosolv sugarcane bagasse lignin in cooperative ionic liquid pairs, Catal. Today 298 (2017) 168–174.
[44] S.F. Hamad, N. Stehling, C. Holland, J.P. Foreman, C. Rodenburg, Low-voltage SEM of natural plant fibers: microstructure properties (surface and cross-section) and their link to the tensile properties, Procedia Engineering 200 (2017) 295–302.
[45] U. Stachewicz, P.K. Szewczyk, A. Kruk, A.H. Barber, A. Czyrska-Filemonowicz, Pore shape and size dependence on cell growth into electrospun fiber scaffolds for tissue engineering: 2D and 3D analyses using SEM and FIB-SEM tomography, Mater. Sci. Eng. C (2017), https://doi.org/10.1016/j.msec.2017.08.076 (in press).
[46] Z. Ning, R. Liu, R.F. Elhajjar, F. Wang, Micro-modeling of thermal properties in carbon fibers reinforced polymer composites with fiber breaks or delamination, Compos. B Eng. 114 (2017) 247–255.
[47] F. Cosmi, A. Bernasconi, Micro-CT investigation on fatigue damage evolution in short fibre reinforced polymers, Compos. Sci. Technol. 79 (2013) 70–76.
[48] Y. Wan, I. Straumit, J. Takahashi, S.V. Lomov, Micro-CT analysis of internal geometry of chopped carbon fiber tapes reinforced thermoplastics, Compos. Appl. Sci. Manuf. 91 (2016) 211–221.
[49] J.C. Ferguson, F. Panerai, J. Lachaud, A. Martin, S.C.C. Bailey, N.N. Mansour, Modeling the oxidation of low-density carbon fiber material based on micro-tomography, Carbon 96 (2016) 57–65.
[50] J. Liu, C. Li, J. Liu, G. Cui, Z. Yang, Study on 3D spatial distribution of steel fibers in fiber reinforced cementitious composites through micro-CT technique, Construct. Build. Mater. 48 (2013) 656–661.
[51] P. Kainourgios, I.A. Kartsonakis, D.A. Dragatogiannis, E.P. Koumoulos, P. Goulis, C.A. Charitidis, Electrochemical surface functionalization of carbon fibers for chemical affinity improvement with epoxy resins, Appl. Surf. Sci. 416 (2017) 593–604.
[52] A. Abrishambaf, M. Pimentel, S. Nunes, Influence of fibre orientation on the tensile behaviour of ultra-high performance fibre reinforced cementitious composites, Cement Concr. Res. 97 (2017) 28–40.
[53] S.Y. Jang, S. Ko, Y.P. Jeon, J. Choi, N. Kang, H.C. Kim, H.-I. Joh, S. Lee, Evaluating the stabilization of isotropic pitch fibers for optimal tensile properties of carbon fibers, J. Ind. Eng. Chem. 45 (2017) 316–322.
[54] J.P. Torres, L.J. Vandi, M. Veidt, M.T. Heiztmann, Statistical data for the tensile properties of natural fibre composites, Data in brief 12 (2017) 222–226.
[55] Y. Zhong, W. Bian, Analysis of the tensile moduli affected by microstructures among seven types of carbon fibers, Compos. B Eng. 110 (2017) 178–184.
[56] B.X. Bie, J.Y. Huang, D. Fan, T. Sun, K. Fezzaa, X.H. Xiao, M.L. Qi, S.N. Luo, Orientation-dependent tensile deformation and damage of a T700 carbon fiber/epoxy composite: a synchrotron-based study, Carbon 121 (2017) 127–133.
[57] S. Borodulina, H.R. Motamedian, A. Kulachenko, Effect of fiber and bond strength variations on the tensile stiffness and strength of fiber networks, Int. J. Solid Struct. (2016), https://doi.org/10.1016/j.ijsolstr.2016.12.013 (in press).
[58] S. Wang, Z. Zhou, H. Xiang, W. Chen, E. Yin, T. Chang, M. Zhu, Reinforcement of lignin-based carbon fibers with functionalized carbon nanotubes, Compos. Sci. Technol. 128 (2016) 116–122.
[59] B. Pang, S. Yang, W. Fang, T.-Q. Yuan, D.S. Argyropoulos, R.-C. Sun, Structure-property relationships for technical lignins for the production of lignin-phenol-formaldehyde resins, Ind. Crop. Prod. 108 (2017) 316–326.
[60] H. Luo, M.M. Abu-Omar, Chemicals from Lignin, in: M.A. Abraham (Ed.), Encyclopedia of Sustainable Technologies, Elsevier Inc., 2017, pp. 573–585.
[61] M. Norgren, H. Edlund, Lignin: recent advances and emerging applications, Curr. Opin. Colloid Interface Sci. 19 (2014) 409–416.
[62] S. Eskandari, F.M. Andrade Pires, P.P. Camanho, A.T. Marques, Intralaminar damage in polymer composites in the presence of finite fiber rotation: Part II – numerical analysis and validation, Compos. Struct. 151 (2016) 127–141.
[63] D. Chen, J. Li, J. Ren, Influence of fiber surface-treatment on interfacial property of poly(l-lactic acid)/ramie fabric biocomposites under UV-irradiation hydrothermal aging, Mater. Chem. Phys. 126 (2011) 524–531.
[64] X. Yan, S. Cao, Structure and interfacial shear strength of polypropylene-glass fiber/carbon fiber hybrid composites fabricated by direct fiber feeding injection molding, Compos. Struct. 185 (2018) 362–372.
[65] Y.-l. Xu, A.Q. Dayo, J. Wang, A.-r. Wang, D. Lv, A. Zegaoui, M. Derradji, W.-b. Liu, Mechanical and thermal properties of a room temperature curing epoxy resin and related hemp fibers reinforced composites using a novel in-situ generated curing agent, Mater. Chem. Phys. 203 (2018) 293–301.
[66] A. Zegaoui, M. Derradji, R.-k. Ma, W.-a. Cai, A. Medjahed, W.-b. Liu, A.Q. Dayo, J. Wang, G.-x. Wang, Influence of fiber volume fractions on the performances of alkali modified hemp fibers reinforced cyanate ester/benzoxazine blend composites, Mater. Chem. Phys. 213 (2018) 146–156.